

<sup>1</sup> INSEAN - Italian Ship Model Basin - Rome, Italy

<sup>2</sup> Lavrentyev Institute of Hydrodynamics - Novosibirsk, Russia

## 1 Introduction

The small time analysis of the starting flow close to the intersection between the liquid surface and a floating wedge is considered. The liquid and the body are initially at rest. At some instant of time taken as the initial one ( $t = 0$ ), the floating wedge with deadrise angle  $\gamma$  impulsively starts to move down with a constant velocity  $V$ . The liquid is assumed ideal and incompressible, and its flow potential. We shall determine both the liquid flow and position of the free surface, which are uniformly valid during the initial stage, where  $Vt/h_0 \ll 1$ ,  $h_0$  is the initial draft of the floating wedge.

The pressure-impulse theory was used by Sedov (1935) to obtain the liquid flow just after the impact instant. Within this theory the boundary conditions are linearised and imposed on the initially undisturbed liquid boundary. The theory predicts the flow singularity at the intersection points. The right-hand side intersection point,  $x = x_c$ ,  $y = 0$ , where  $x_c = h_0 \cot \gamma$ , is considered below. In a small vicinity of this point,  $r/h_0 \ll 1$ , the velocity potential  $\phi(x, y, t)$  behaves like (Iafrazi & Korobkin 2000)

$$\phi \simeq -Ar^{\sigma_0} \cos(\sigma_0\theta) , \tag{1}$$

where  $\sigma_0 = \pi/(2\beta)$ ,  $\beta = \pi - \gamma$  and  $(r, \theta)$  are the cylindrical coordinates with the origin at the intersection point (see figure 1). The coefficient  $A$  depends on the entry velocity  $V$ , the deadrise angle  $\gamma$  and the initial draft  $h_0$ . Here  $\frac{1}{2} < \sigma_0 < 1$ , which implies that the solution by Sedov predicts non-physical behavior of the flow close to the intersection point and has to be considered as the first-order 'outer' solution. The higher-order 'outer' solution can be derived using the small-time expansion procedure. In order to obtain uniformly valid description of the flow during the initial stage, an 'inner' solution must be considered within stretched variables.

It is shown that in the leading order as  $Vt/h_0 \rightarrow 0$  the inner solution is non-linear, self-similar and depends only on the wedge deadrise angle  $\gamma$ . Deflection of the inner free surface cannot be neglected even in the leading order in contrast to the Sedov's solution. The solution of the inner problem is achieved by decomposing the fluid domain in three parts: the far-field region, the intermediate region and the jet region. Asymptotic methods are used to evaluate both the shape of the free surface and the velocity potential in the far-field region. The flow in the jet region is described within the shallow-water approximation. The solution in the intermediate region is determined numerically by iterations. A boundary integral representation is used for the velocity potential. Shape of the free surface in the intermediate region is obtained using a pseudo-time stepping procedure developed. The shallow-water solution in the jet region is updated at each step of the iterations and is directly incorporated into the solution of the boundary-value problem in the intermediate region. It is shown that the developed procedure is stable and provides the combined numerical-asymptotic solution of the inner problem with a given accuracy.

## 2 Formulation of the inner problem

The starting flow close to the intersection point  $x = x_c$ ,  $y = 0$  is considered with the help of the stretched non-dimensional variables

$$x = x_c + a(t)\lambda, \quad y = a(t)\mu, \quad \phi(x, y, t) = Aa^{\sigma_0}(t)\varphi(\lambda, \mu, t), \quad a(t) = [(2 - \sigma_0)At]^{\frac{1}{2-\sigma_0}}. \tag{2}$$

Substituting (2) into the original equations and the boundary conditions, we obtain that in the leading order as  $a(t)/h_0 \rightarrow 0$  the inner flow is quasi-stationary,  $\varphi \approx \varphi(\lambda, \mu)$ , and the entry velocity can be neglected compared to velocity of the flow close to the intersection point.

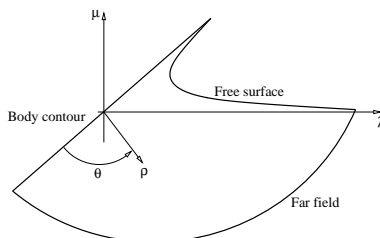


Figure 1: Sketch of the inner region for the small-time analysis.

It is convenient to introduce the modified velocity potential  $S = \varphi - \frac{1}{2}\rho^2$ , where  $\rho = \sqrt{\lambda^2 + \mu^2}$ , which satisfies the following equations (Iafrati & Korobkin 2000)

$$\nabla^2 S = -2 \quad \text{in the flow region,} \quad (3)$$

$$S_n = 0 \quad \text{along both the free surface and the wedge surface,} \quad (4)$$

$$S_\tau^2 + 2\sigma_0 S = (1 - \sigma_0)\rho^2 \quad \text{along the free surface,} \quad (5)$$

$$S \simeq -\frac{1}{2}\rho^2 - \rho^{\sigma_0} \cos(\sigma_0\theta) \quad (\rho \rightarrow \infty), \quad (6)$$

where  $S_n$  and  $S_\tau$  are the normal and tangential derivatives of the unknown function  $S(\lambda, \mu)$  on the boundary. The far-field condition (6) follows from matching the 'inner' solution (2) and the 'outer' solution (1). Therefore, in the leading order the flow near the intersection point is self-similar and depends only on the parameter  $\sigma_0$ .

The inner problem (3) - (6) is non-linear and complicated. Moreover, the shape of the free surface is unknown in advance and has to be determined together with the liquid flow. If the free surface is known, the dynamic boundary condition (5) can be integrated providing the velocity potential along the free surface and, therefore, the velocity field throughout the inner flow region in quadratures.

### 3 Asymptotic behavior of the inner solution in the far field

In order to reduce the size of the computational domain required to solve the inner problem (3) - (6), the asymptotic behavior of the solution in the far field is estimated. It should be noted that the Stokes' procedure does not work in this case and we have to map the far-field region onto a canonical one to find the asymptotic expansion of the modified potential  $S(\lambda, \mu)$ . The free-surface shape in the far field is described by the equation  $\theta = \tilde{\theta}(\rho)$ , where  $\tilde{\theta}(\rho) \rightarrow \beta$  as  $\rho \rightarrow \infty$ . It is useful to introduce the new angular variable  $\alpha = \theta\beta/\tilde{\theta}(\rho)$  so that the fluid domain in the far field corresponds to  $0 \leq \alpha \leq \beta$ . Three cases are distinguished: (i)  $\gamma > \pi/4$ , (ii)  $\gamma = \pi/4$  and (iii)  $\gamma < \pi/4$ . In the case  $\gamma > \pi/4$ , we obtain

$$\begin{aligned} \tilde{\theta}(\rho) &= \beta + \frac{\sigma_0}{2 - \sigma_0} \rho^{\sigma_0 - 2} - \frac{\sigma_0^2(1 - \sigma_0)}{2(2 - \sigma_0)^2} \tan(2\gamma) \rho^{2\sigma_0 - 4} + o(\rho^{2\sigma_0 - 4}), \quad \theta = \alpha \frac{\tilde{\theta}(\rho)}{\beta}, \\ S(\rho, \theta) &= -\frac{1}{2}\rho^2 - \rho^{\sigma_0} \cos(\sigma_0\alpha) + \frac{\sigma_0^2}{2 - \sigma_0} \left[ \frac{\alpha}{\beta} \sin(\sigma_0\alpha) + \frac{\cos[2(1 - \sigma_0)\alpha]}{2 \cos(2\gamma)} \right] \rho^{2\sigma_0 - 2} + o(\rho^{2\sigma_0 - 2}), \\ S(\rho, \tilde{\theta}(\rho)) &= -\frac{1}{2}\rho^2 + \frac{\sigma_0^2}{2(2 - \sigma_0)} \rho^{2\sigma_0 - 2} - \frac{\sigma_0^3(1 - \sigma_0)}{2(2 - \sigma_0)^2} \tan(2\gamma) \rho^{3\sigma_0 - 4} + o(\rho^{3\sigma_0 - 4}). \end{aligned} \quad (7)$$

The corresponding expansions for the blunt-wedge case,  $\gamma \leq \pi/4$ , have been also derived. They are more complicated than expansions (7) due to eigensolutions, orders of which are comparable with the orders of other terms appeared in the expansions.

### 4 Mass conservation

The inner solution has to be determined in the unbounded region, whose shape is unknown in advance. The matching condition (6) shows that the mass flux incoming into the inner flow domain from the outer region is infinite. This infinite flux has to be balanced in some sense by deflection of the free surface in the inner region and by the mass outflow through the jet. In order to understand better the mechanism of this balance, let us consider a point  $E$  located on the free surface in the far-field region and a point  $F$  located on the free surface in the jet region. We consider the finite part  $\mathcal{D}_{EF}$  of the flow domain, which is bounded in the far field by the circumference  $\rho = R_E$ , in the jet region by a straight line orthogonal to the body contour through the point  $F$ , on the top by the free surface and on the left-hand side by the body contour. Equation (3) gives

$$\int_{\mathcal{D}_{EF}} \nabla^2 S \, d\lambda d\mu = \int_{\partial\mathcal{D}_{EF}} \frac{\partial S}{\partial n} \, ds = -2|\mathcal{D}_{EF}|,$$

where  $|\mathcal{D}_{EF}|$  is the area of the finite region  $\mathcal{D}_{EF}$ . According to the boundary conditions (4) on the free surface and on the body contour, the normal derivative of  $S$  differs from zero only along the far-field boundary and on the jet cut at  $F$ . When  $E$  tends to infinity both the mass flux from the far-field boundary and the area  $|\mathcal{D}_{EF}|$  are unbounded. However, with the help of the asymptotic expansions (7), it can be shown that the two contributions balance each other for any finite  $R_E$ , thus leading to a finite flux of mass through the jet cut.

Concerning the behavior of the solution in the jet region, there are two possibilities: (i) the jet is of finite length and (ii) the jet is of infinite length. Whatever is the case, we assume that the fluid flows from the intermediate region into the jet region through the cut  $F$ . In order to satisfy both the kinematic condition on the free surface and the

body boundary condition (4) in the case of finite length of the jet and a non-zero angle at the jet tip, it must be  $S_\tau(0) = 0$ , where  $\tau$  is the coordinate along the free surface with  $\tau = 0$  at the jet tip. By differentiating the dynamic boundary condition (5) with respect to  $\tau$ , we obtain

$$\lim_{\tau \rightarrow 0^+} \frac{S_\tau^2(\tau) - S_\tau^2(0)}{\tau} = 2(1 - \sigma_0)\rho\rho_\tau(0) - 2\sigma_0 S_\tau(0).$$

Since  $S_\tau(0) = 0$ , the left-hand side is positive and the equality implies  $\rho_\tau(0) > 0$ . On the other hand,  $\varphi_\tau(0) = S_\tau(0) + \rho(0)\rho_\tau(0) > 0$ , which shows that in this case the liquid particles move in the jet region from the jet tip. This result contradicts to the assumption about the flow pattern in the jet region. Therefore, infinite length of the jet is expected.

## 5 Asymptotic behavior of the inner solution in the jet region

Asymptotic analysis of the flow in the thin jet region is carried out by using ideas from the shallow-water theory. It is convenient to introduce the new Cartesian coordinate system  $O\xi\eta$  with the axis  $O\xi$  directed along the body surface and the axis  $O\eta$  towards the liquid region. The jet cut  $F$  is given now as  $\xi = \xi_0$ ,  $0 < \eta < h(\xi_0)$ , where equation  $\eta = h(\xi)$  describes the free-surface shape in the jet region,  $\xi \geq \xi_0$ . Within the stretched variables  $\eta = h(\xi)z$ ,  $h(\xi) = h(\xi_0)T(\xi)$  and  $s(\xi, z) = S(\xi, h(\xi)z)$  the jet region corresponds to the strip,  $\xi \geq \xi_0$ ,  $0 < z < 1$ , and the unknown functions  $T(\xi)$  and  $s(\xi, z)$  can be found in the forms  $T(\xi) = T_0(\xi) + h^2(\xi_0)T_1(\xi) + \dots$  and  $s(\xi, z) = s_0(\xi, z) + h^2(\xi_0)s_1(\xi, z) + \dots$ , where  $h^2(\xi_0)$  is considered as a small parameter. Substituting these asymptotic expansions into (3) - (6), we obtain

$$\begin{array}{llll} \text{Eq. (3)} & s_{0zz} = 0, & s_{1zz} = -2T_0^2 - T_0^2 s_{0\xi\xi} & 0 < z < 1 \\ \text{KBC (4)} & s_{0z} = 0, & s_{1z} = T_{0\xi}T_0 s_{0\xi} & z = 1 \\ \text{BBC (4)} & s_{0z} = 0, & s_{1z} = 0 & z = 0 \\ \text{DBC (5)} & s_{0\xi}^2 = (1 - \sigma_0)\xi^2 - 2\sigma_0 s_0, & 2s_{0\xi}s_{1\xi} = (1 - \sigma_0)T_0^2 - 2\sigma_0 s_1 + T_{0\xi}^2 [(1 - \sigma_0)\xi^2 - 2\sigma_0 s_0] & z = 1 \end{array}$$

in the leading and for the second order, respectively. The system of the differential equations is numerically solved with a space-marching procedure for  $\xi > \xi_0$ , starting from  $\xi_0$  and a given thickness  $h(\xi_0)$  provided by the solution in the intermediate region.

## 6 Numerical solution in the intermediate region

In order to solve completely the inner problem, the numerical iterative procedure is developed to find the shape of the free surface in the intermediate region. Both the inner potential  $\varphi$  and the modified potential  $S$ , where  $\varphi = S + \frac{1}{2}\rho^2$ , are used. The inner potential  $\varphi$  satisfies the Laplace equation, solution of which is sought by using a boundary integral formulation in the computational domain bounded by the far-field boundary, the body contour and the free surface. The far field boundary ( $FF$ ) is located at  $\rho = R$  with  $R$  being large enough so that the asymptotic expansion (7) is expected to represent the solution with a given accuracy for  $\rho \geq R$ . The same expansion is used also to assign the value of the velocity potential along the far-field boundary.

The main issue is related to the free surface ( $FS$ ) shape that is unknown and must be determined as a part of the solution. To this aim a pseudo time-stepping procedure is adopted by using the asymptotic expansion (7) as a first guess. Once the free surface shape is assigned, the distribution of the velocity potential along the free surface is obtained by integrating the dynamic boundary condition (5), which is rewritten as  $S_\tau = -\sqrt{(1 - \sigma_0)\rho^2 - 2\sigma_0 S}$ , and then using the relation  $\varphi = S + \rho^2/2$ . On the wetted part of the body contour ( $BC$ ) the impermeability condition,  $\partial\varphi/\partial n = 0$ , is applied.

The solution of the boundary-value problem provides the velocity potential along the wetted part of the body and its normal derivative along both the free surface and the far-field boundary. This allows us to compute  $\nabla S$  on the free surface and to verify then if the kinematic boundary condition,  $\partial S/\partial n = 0$ , is satisfied. If not, the free surface shape is updated by using  $\nabla S$  as a free-surface velocity. Special treatment of the intersection between the free surface and the body contour is required. The angle at the intersection progressively decays and, when it drops below a limit value, the jet is cut off and is replaced by the jet region, where the flow is described within the shallow-water approximation (see section 5). In this way we obtain the shape of the free surface and the distribution of the velocity potential along both the body contour and the free surface. The shallow-water ( $SW$ ) part is directly included into the boundary integral formulation. In order to clarify the numerical procedure, the boundary integral representation is written for a point  $\mathbf{x}$  on the boundary of the computational domain, which leads to the following boundary integral equation

$$\begin{aligned} \frac{1}{2}\varphi(\mathbf{x}) + \int_{BC} \varphi(\mathbf{y}) \frac{\partial G}{\partial n}(\mathbf{x} - \mathbf{y}) ds(\mathbf{y}) - \int_{FS \cup FF} \frac{\partial \varphi}{\partial n}(\mathbf{y}) G(\mathbf{x} - \mathbf{y}) ds(\mathbf{y}) = & \quad (8) \\ \int_{BC \cup SW} \frac{\partial \varphi}{\partial n}(\mathbf{y}) G(\mathbf{x} - \mathbf{y}) ds(\mathbf{y}) - \int_{FS \cup FF \cup SW} \varphi(\mathbf{y}) \frac{\partial G}{\partial n}(\mathbf{x} - \mathbf{y}) ds(\mathbf{y}), & \end{aligned}$$

where the Cauchy principal value of the integral is taken for the singular ones. It must be noted that for  $\mathbf{x} \in FF \cup FS$  the velocity potential is assigned and the first term on the left-hand side of (8) is moved to the right-hand side of the equation.

In Fig. 2 a close up view of the region about the matching between the intermediate region and the shallow water part is shown. On the left picture the geometry is shown whereas the distribution of the modified velocity potential versus  $\lambda$  is shown on the right. In both cases the transition between the two regions is very regular.

Two different checks were performed to evaluate the convergence of the solution and its accuracy (Fig. 3). The integral of  $(\partial S/\partial n)^2$  along the free surface can be regarded as a measure of the accuracy at which the kinematic boundary condition is satisfied. Moreover, the area enclosed between the disturbed free surface and its initial level,  $\mu = 0$ , is computed and compared with the incoming flow from the far field boundary, in order to check the mass conservation. Results show that convergence is achieved after about 1500 iterations (Fig. 3).

Finally, calculations are performed by varying the far field extension of the computational domain ( $R = 40$  and 28) and different values of the limit angle ( $10^\circ$  and  $5^\circ$ ) for the matching with the shallow-water solution. In both cases results show that the solution is essentially independent of those parameters (see Fig. 4), provided they are properly chosen so that the corresponding asymptotic expansions hold.

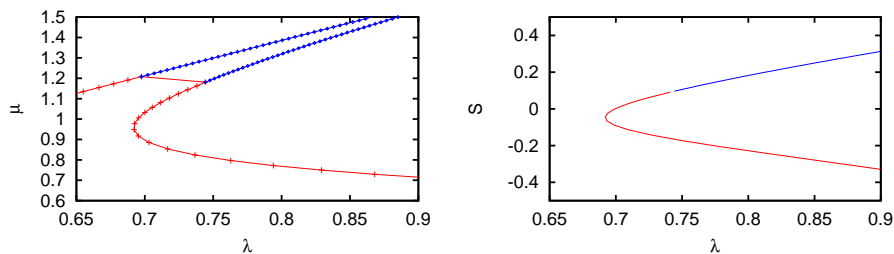


Figure 2: Close up view of the region about the matching between the intermediate region and the shallow water part. ( $\gamma = 60^\circ$ )

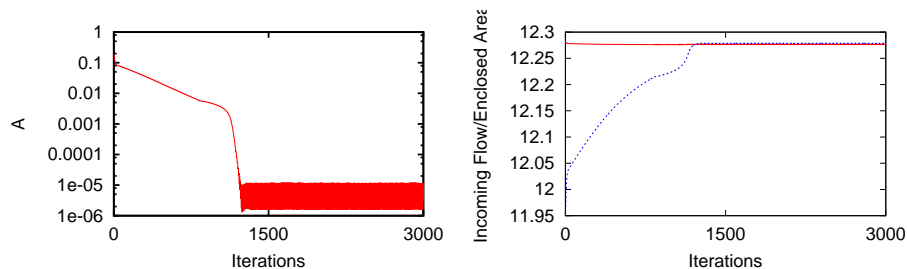


Figure 3: left) Integral of  $(\partial S/\partial n)^2$  along the free surface; right) Incoming flow and area enclosed by the free surface.

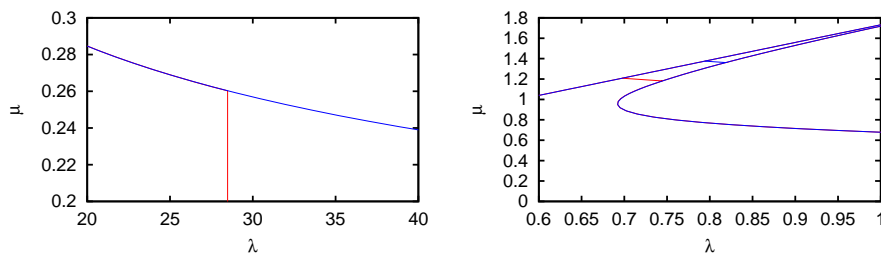


Figure 4: left) Solutions obtained with two different extension of the computational domain are compared close to the end of the shorter domain; right) Solutions obtained by using two different values of the limit angle for the cut of the jet are compared in the matching region.

## Acknowledgments

A.A.K. acknowledges the support from RFBR (projects No. 00-01-00839 and No. 00-15-96162) and SB RAS (integrated grant No. 1). A.I. acknowledges the support from *Ministero dei Trasporti e Navigazione* in the framework of the INSEAN research plan 2000-02.

## References

- SEDOV, L.I.: *Floating wedge impact*, Tr. Tsentr. Aerodin. Inst., 152, pp. 27-31 (1935).  
 IAFRATI, A., KOROBKIN, A.A.: *Liquid flow close to intersection point*, Proc. 15th Workshop on Water Waves and Floating Bodies, (2000).